



1

1 **Balloon drift estimation and improved position estimates for** 2 **radiosondes**

3 Ulrich Voggenberger¹, Leopold Haimberger¹, Federico Ambrogi¹, Paul Poli²

4 ¹Department of Meteorology and Geophysics, University of Vienna, Vienna, 1090, Austria

5 ²European Centre for Medium-Range Weather Forecasts, Bonn, Germany

6 *Correspondence to:* Ulrich Voggenberger (ulrich.voggenberger@univie.ac.at)

7 **Abstract.**

8 When comparing model output with historical radiosonde observations, it is usually assumed that the radiosonde has risen
9 exactly above its starting point and has not been displaced by the wind. This has changed only relatively recently with the
10 availability of Global Navigation Satellite System (GNSS) receivers aboard the radiosondes in the late-1990s, but even then
11 the balloon trajectory data were often not transmitted, although this information was the basis for estimating the wind in the
12 first place. Depending on the conditions and time of year, radiosondes can sometimes drift a few hundred kilometres,
13 particularly in the mid-latitudes during the winter months. The position errors can lead to non-negligible representation
14 errors when the corresponding observations are assimilated.

15 This paper presents a methodology to compute changes in the balloon position during its vertical ascent, using only limited
16 information, such as the vertical profile of wind contained in the historical observation reports. The sensitivity of the method
17 to various parameters is investigated, such as the vertical resolution of the input data, the assumption about vertical ascent
18 speed of the balloon, and the departure of the surface of the Earth from a sphere. The paper considers modern GNSS sonde
19 data reports for validation, for which the full trajectory of the balloon is available, alongside the estimated wind. Evaluation
20 is also conducted by comparison with ERA5 and by conducting low-resolution data assimilation experiments. Overall, the
21 results indicate that the trajectory of the radiosonde can be accurately reconstructed from original data of varying vertical
22 resolution and that the more accurate balloon position reduces representation errors, and, in some cases, also systematic
23 errors.

2
3



4

24 **1 Introduction**

25

26 Prior to the availability of remote sensing techniques, upper-air measurements of air motions were widely collected using
27 Lagrangian perspectives, with weather balloons (e.g., Dutton, 1986). The uncertainty of such upper air observations depends
28 not only on the measurements themselves but also on the availability and quality of associated metadata and measurement
29 position: this is generally associated with so-called representativeness errors (e.g., Kitchen, 1989). As weather balloons drift
30 with the wind during their travel, including ascent, they can thus be displaced over large distances, in some cases more than
31 400 km from their launch base (e.g., Seidel et al., 2011). Precise knowledge of the balloon position is particularly important
32 in regions of steep horizontal gradients, e.g. near mountain ranges or near jet streams. Tschannett (2003) and Steinacker et al.
33 (2005) noted that apparent superadiabatic vertical lapse rates in Foehn events disappeared after the balloon displacement had
34 been taken into account. For operational monitoring, detailed information regarding the balloon trajectory was generally not
35 recorded or not transferred via the data distribution networks until the advent of Global Navigation Satellite Systems
36 (GNSS). Even later, when GNSS sensors became available, the information collected was often not transmitted, although the
37 wind data was calculated directly from it (WMO, 2021). Only since the mid-2010s is the balloon drift taken into account in
38 modern observation processing of GNSS sondes, with beneficial results (Ingleby, 2018).

39

40 Radiosonde measurements are used in a variety of applications, including near-real-time by forecasters and Numerical
41 Weather Prediction (NWP), but also for air pollution or other scientific investigations, including climate monitoring (e.g.,
42 Dabberdt and Turtiainen, 2015). The production of climate reanalyses that directly assimilate radiosonde observations, such
43 as ERA5 (Hersbach et al. 2020), is expected to benefit from more accurate historical balloon position data, similarly to
44 NWP. In this regard, the location precision of the assimilated measurements should be commensurate with the horizontal
45 resolution (~10 to 20 km globally) of future reanalyses. At such resolutions, assuming vertical ascents for a balloon that is
46 displaced by a couple of hundred kms would amount to comparing the balloon measurements with model values that are 10
47 or more grid boxes away, which is clearly suboptimal. Resolving this situation requires, for historical soundings, to
48 reconstruct the balloon trajectories from the little information that is available (Stohl, 1998). In many cases, this information
49 only consists in the vertical profile of wind, as discussed later in the paper.

51 The present paper presents a method to calculate the balloon drift from historical radiosonde ascent data. Section 2 describes
52 the data and methodology. Details of the technical implementation, with python code and test data, are provided in section 3.
53 Section 4 presents verification results including from several sensitivity analyses to explore the robustness and accuracy of
54 the approach. Sections 5 and 6 show evaluation results, using two different approaches, whereby the beneficial impact of the
55 more accurate balloon position is demonstrated. Section 7 includes a discussion and conclusions.

5

6



7

56 **2 Data and methodology**

57

58 **2.1 Radiosonde data**

59 Radiosonde data used in this work are obtained from the Integrated Global Radiosonde Archive (IGRA), Version 2 (Durre et
60 al., 2016) and via the Copernicus Climate Change Service (C3S) Climate Data Store (CDS). High-resolution radiosonde data
61 used for verification are obtained in BUFR (Binary Universal Form for the Representation of meteorological data) format
62 from the University of Wyoming Atmospheric Science Radiosonde Archive (UWYO).

63

64 The quality of the available wind data depends on their encoding and the method used to track the balloons. Measuring
65 techniques for upper air winds have changed significantly over time, with a clear general trend towards improvements in
66 quality, thanks to removal of procedural errors, in particular (e.g., Crutcher, 1979), noting also improvements in the accuracy
67 of encoding, with evolution of the data formats. All these changes are described in the WMO Publication Nr. 8, Guide to
68 Meteorological Instruments and Methods of Observation, published since 1954 by the WMO Commission for Instruments
69 and Methods of Observation (CIMO; WMO, 2021). Regarding changes in the measurements of wind and balloon positions,
70 there are three important distinctions to be made.

71

72 The first distinction concerns the sensing apparatus: non-GNSS versus GNSS sondes. The latter sondes can track the
73 horizontal and vertical position of the balloon and the sensor at high frequency, thanks to improvements and miniaturisation
74 of the electronics. The resulting data are then used to calculate the wind variable in the data set. Early observations used only
75 ground-based tracking, e.g., by theodolite, which was fairly accurate but could lose the balloon early during cloudy or strong
76 wind conditions, and relied on an assumed ascent rate if a single theodolite was used (e.g., Favà et al., 2021). From the mid-
77 1950s onward, radar tracking or radio-positioning of the radiosonde became standard. In the 1990s, GNSS modules were
78 introduced, but the position data were not transmitted to the global network and are therefore not available in the used input
79 data bases in most cases until 2014.

80

81 The second aspect is the determination of altitude. Prior to GNSS observations, altitude was determined by three different
82 methods: ascent speed estimation, pressure sensors and vertical radar or radio-positioning, with continued efforts to increase
83 the quality of observations over time. Ascent speed can be affected by many factors, and Murillo et al. (2005) estimated a
84 scatter in linear ascent rates of about 5% about the mean value for pilot balloons, after using double theodolites to conduct
85 measurements to measure the balloon height during ascent.

86

8

9



10

87 The third aspect is the data format used for transmission. Essentially two main message systems have been used to transmit
88 the observed radiosonde data: Traditional Alphanumeric Code (TAC) and BUFR. The main difference is that the latter not
89 only has a much higher vertical resolution (1 second frequency, corresponding to approximately 5 m altitude), but also a
90 higher coding precision. The BUFR messages report wind direction with a resolution of 1 degree, whereas TAC messages
91 report wind direction to the nearest 5-degree. TAC messages typically also include data only on mandatory and significant
92 levels. Mandatory levels are a set of predefined pressure levels. Significant levels are added as needed before transmission so
93 that the wind speed does not deviate by more than 5 m/s from linearly-interpolated values, according to the above-cited
94 WMO CIMO guide.

95

96 **2.2 Quality control**

97 The following steps are taken to exclude outliers:

- 98 ● The wind speed is limited to 150 m/s, a value that is rarely reached, even in strong upper-level jets.
- 99 ● The temperature is limited to values between 173 K and 373 K.

100 Observations that fall outside these limits are not processed further, to avoid degrading the quality of the output (balloon
101 trajectory).

102

103 **2.3 Estimation of the balloon trajectory**

104 The balloon position is calculated relative to the launch position (so-called base coordinates), as latitude displacement and
105 longitude displacement (decimal degrees). For each vertical level, these two values can be added to the base coordinates to
106 obtain the new (latitude, longitude) position at the given level. The same approach applies to the reconstruction of the
107 measurement times at all levels. This practice conforms to the BUFR encoding standard.

108

109 For the position calculation, the same simple physical laws that have been used to derive the reported winds are applied.
110 Only a few initial parameters are necessary for this:

111

- 112 ● station coordinates or starting point of the sonde, here called base coordinates (latitude and longitude);
- 113 ● wind vector (zonal and meridional components, noted respectively u and v), measured by the sonde at different
114 pressure levels;
- 115 ● measurement time (t) at different pressure levels.

116

117 These variables enable calculation of how long the sonde was exposed to horizontal wind, and therefore can be used to
118 estimate the displacement of the sonde.

11
12



13

119 Especially older datasets often only contain the starting time of the ascent, but temporal information is not available for all
120 the reported pressure levels.

121 To estimate the time elapsed since the release of the balloon, two variables are needed:

122

- 123 ● the reported pressure levels (generally available from radiosondes) or heights (generally available from so-called
124 PILOT balloons, also called PIBAL),
- 125 ● the sonde ascent speed.

126

127 PILOT or PIBAL profiles provide an estimate of height at each level, from which the time at each level can be reconstructed,
128 assuming a given ascent speed. However, for multivariate soundings (radiosondes reporting temperature and wind), observed
129 pressure is often the only information available regarding the radiosonde vertical position. In such a case, the pressure profile
130 needs to be transformed to a height profile. This can be done assuming a piecewise polytropic atmosphere, using the
131 available temperature profile. The calculation of the vertical gradient of temperature with respect to altitude from the vertical
132 gradient of temperature with respect to pressure is shown below in **Formula 1** and **2**. Subsequently, **Formula 3** indicates
133 how this information is used to determine the heights of all pressure levels. If the height information is already available (e.g.
134 PILOT data), those steps can be skipped.

135

136 The vertical resolution of the available data varies. While early ascents often contain even less than the mandatory levels (16
137 levels), recent data in high resolution BUFR are available on 3000 and more levels. The sensitivity of displacement
138 calculations to vertical resolution is investigated later in this paper.
139 If a single mandatory level is missing within the ascent range, then the displacements are not calculated; we consider that too
140 much information is missing in such a case. If a level was not mandatory in historical data (e.g. 70 hPa, 250 hPa, 925 hPa),
141 this rule does not apply to the data. However, an early termination of the vertical ascent is not an issue, then the
142 displacements are only calculated up to the highest available level.

143

144 The determination of the sonde's ascent speed is more uncertain. It depends on some variables that are poorly determined or
145 unknown, such as the air vertical wind speed and the weight to buoyancy ratio of the probe and the balloon. Deviations in the
146 filling level of the balloon, the air resistance of the balloon skin, as well as the ambient temperature and the balloon gas
147 temperature further influence the ascent speed. A review of some of these factors was made by Favà et al. (2021).

148

149 Using data from recent sondes, our study of the data with known altitude time series indicates that the rate of ascent varies
150 mostly between 2 and 10 m/s. Within this large range, **Figure 2** shows that the mode of the distribution of ascent speeds is
151 around 5 m/s. **Table 3** further indicates that the interquartile range is 2 m/s (i.e., from 4 m/s to 6 m/s). These findings are

14
15



16

152 consistent with other sources (e.g., Seidel et al., 2011). These statistics represent global fluctuations in the ascent speed of
153 weather balloons.

154

155 Over short time scales, **Figure 3** indicates the vertical velocity of the probe fluctuates substantially. This is true for the
156 differences within a single ascent, but also for the differences between different ascents. Near the ground and above the
157 tropopause the fluctuations are largest.

158

159 Given the considerations above for historical balloons, one must recognize that the vertical speed can only be estimated in
160 most cases, and will always lead to significant deviations as compared to measurements obtained from high resolution
161 ascents. Note the high vertical resolution shown in **Figure 3** is hardly reached in ascents before the year 2000. This also
162 means that if only mandatory levels are available, the fluctuations in average ascent speed at each available level are
163 smaller, due to the longer averaging intervals.

164

165 **Figure 2** and **Figure 3** show that an assumed ascent rate of 5 m/s agrees well with the observed mean value. To counteract
166 the effects of this fluctuating parameter, an attempt was made to use a height-dependent function instead of a constant speed,
167 which represents the annual average over more than 100 stations.

168

169 As part of this experiment, a polynomial model was also used to improve the accuracy of the average ascent speed. The
170 resulting displacements showed, however, very little improvement, indicating that the assumed vertically constant ascent rate
171 of 5 m/s is a sufficient approximation.

172

173 As a next step it is necessary to calculate the height profile from temperature and pressure information using the dry
174 polytropic height formula (Alexander, P., 2011). Relative humidity could also be considered by using the virtual
175 temperature, but, since it is often not available for early ascents and the differences in resulting displacements are small, the
176 air temperature is used in the equation of state. For the first level, the International Civil Aviation Organization (ICAO)
177 standard atmosphere lapse rate of -0.0065 K/m is used. For all subsequent steps, the temperature gradient is calculated
178 directly from the temperature and pressure profile (mean values for each layer “i”).

179

180 The height profile is then used to calculate the time interval spent by the sonde between the noted levels. It can be estimated
181 using the estimated vertical velocity mentioned earlier.

182 These time intervals are then used to determine the transport of the balloon according to the mean wind inside the layer
183 between the levels i to $i+1$, see **Formula 4**.

184

17
18



19

185 Afterwards, this distance is converted into latitude and longitude using either the inverse Haversine method on an assumed
186 sphere, or the forward transport function on the "WGS84" ellipsoid. The difference between the two transport functions is
187 found to be practically invisible for smaller observed displacements (see **Figure 4**). Nevertheless, the ellipsoid option is used
188 as it should deliver higher accuracy results. Finally, the resulting latitudes and longitudes are subtracted from the base
189 coordinates to obtain the displacements.

190

191 **3 Implementation and availability**

192 The software necessary for the creation of calculated balloon trajectories can be found in:

- 193 ● <https://zenodo.org/record/8421009>
- 194 ● <https://pypi.org/project/rs-drift/>
- 195 ● https://github.com/UVoggenberger/rs_drift/

196 Examples on how to use it are available in all repositories as an IPython notebook "rs_drift_example.ipynb".

197

198 In addition to the coordinates of the launch site or station in degrees latitude and longitude, the trajectory function requires
199 profiles of four input variables: temperature [K], pressure [Pa], zonal wind (u) [m/s], meridional wind (v) [m/s]. It accepts
200 only input which is sorted in ascending order.

```
201 trajectory = rs_drift.drift.trajectory(lat,lon,temperature,u,v,pressure)
```

202 The function returns the following output:

```
203 trajectory == [latitude_displacement, longitude_displacement, seconds_since_start]
```

204 All those output variables are numpy arrays, with one element for each pressure level - with the same length as the input
205 data.

206

207 It is possible to experiment with input data. If humidity information is available, the virtual temperature can be used instead
208 of the observed air temperature. Also if more information of the balloon's mean ascent rate is present, this should be used as
209 input in the additional arguments. Any approach including proper quality control of input data that is available should be
210 used to create the best possible estimation of the balloon drift.

211

212 The drift of the balloon and sonde compounds is introduced as "displacement" from the starting point (launch site). For
213 simplicity, the displacements can be added to the base coordinates to obtain the vertical profile of positions of the balloon.

214



22

215 4. Verification with GNSS radiosondes

216 Verification per se is only possible when a trusted source can provide an indisputable reference. Such is the case for modern
217 sondes equipped with GNSS receivers, when it comes to the recovery of the balloon trajectories. For pre-GNSS radiosondes,
218 a similar verification would be possible, if only one had available the information about the balloon trajectory.
219 Unfortunately, this information is available only in rare cases.

220

221 The data from the modern GNSS radiosonde data encoded in the recent high-resolution BUFR files are used to verify the
222 systematic and random errors of the calculated displacements at different pressure levels. This data set contains second-by-
223 second records of actual positions of the sonde measured by GNSS in the form of displacements, thus enabling the direct
224 comparison with the calculated displacements.

225

226 **Figure 4** also shows that the displacements obtained from GNSS and the displacements calculated from the wind data agree
227 quite well. The small deviations likely come from differences between the actual (unknown) and assumed (5 m/s) ascent
228 rate.

229

230 **Figure 5** provides an overview how large the displacements typically are and gives profiles of uncertainty estimates for the
231 calculated displacements. In the troposphere the RMSE is mostly below 0.02 degrees (2.5 km), in the stratosphere it can be
232 up to 0.1 degrees (12 km). These numbers amount to uncertainties of about one part in five to ten, of the observed variations
233 (RMS), in the example shown. Still, this is much better than just ignoring the displacement.

234

235 These results were obtained by using as input the high-resolution data. For historical radiosondes, only comparatively low-
236 resolution information is available (in the form of mandatory plus significant levels).

237 In **Figure 6** and **Figure 7**, the impact of using only mandatory and significant level information is shown. The difference of
238 displacements in **Figure 6** is minimal, although the displacement is relatively large.

239 **Figure 7** shows a case of larger differences in relative terms. The overall longitudinal displacements are large and the winds
240 vary strongly with altitude. Poor representativity of the selected levels - i.e. data points from the high resolution BUFR
241 dataset, far off the mean, may lead to worse results than wind averages between the levels from less high resolution data -
242 see v component of wind original and on mandatory pressure levels only. The method of calculating the displacements itself
243 uses mean wind speeds within the considered levels. Thus, if the observations are also means of larger vertical height
244 differences, more or less randomly observed peaks become a smaller source of error.

245

246 **Figure 8** shows the comparison between the displacements of two different data sets - on high resolution BUFR levels and
247 on the other hand on mandatory levels only. It can be seen that for this subset of ascents there is still much value in the

23
24



25

248 displacements for the mandatory levels only version. However, it should be noted that more available levels always lead to
249 better results and the highest possible number should be used in any case.

250

251 Many of the older observational reports contain temperature and wind data on different levels. Only at mandatory levels both
252 variables are available. In this case, interpolation can be performed for the points in between. When applied to IGRA data,
253 wind data are interpolated to temperature observations. This allows the input to be maximised to calculate the best possible
254 displacements.

255

256 **5. Evaluation with ERA5**

257 To evaluate the impact of taking the displacements into account, we compared the observed values from the radiosondes
258 with the gridded ERA5 data, in one case assuming a strictly vertical ascent, and in the other case assuming an ascent along
259 the calculated (slanted) trajectory defined by the displacements. The ERA5 fields at hourly resolution were used at $1^\circ \times 1^\circ$
260 horizontal resolution, which were then interpolated linearly horizontally to the observations locations defined in either of the
261 two cases mentioned earlier (vertical or slanted).
262 These tests and comparisons used the short term forecast of the ERA5 assimilating model, also referred to as "background".
263 This choice, instead of using ERA5 analyses, was made to try to maintain as much independence as possible with respect to
264 the observations. This choice should largely avoid possible problems resulting from the fact that the observations are also
265 assimilated into the ERA5 data, given that many other observations were assimilated alongside radiosondes and also
266 influenced the analysis state. Experimental comparisons to the ERA5 analyses showed that the analysis data fits significantly
267 better with the vertical trajectory of observation than with the slanted version. This is to be expected, since radiosondes were
268 assimilated as vertical profiles in ERA5.

269

270 **Figure 9** shows the benefit of comparing the radiosonde observations with the background as slanted profiles instead of
271 vertical profiles. In low layers (below 700 hPa), the displacements are relatively smaller than at higher levels, and therefore
272 hardly lead to deviations for temperature. In most cases, there is an improvement at levels located above 750 hPa, though at
273 some stations the improvement is visible already as soon as the sonde reaches 850 hPa, depending on the wind speed and
274 topography around the station. Typically, the effect is largest in regions with high upper-level wind speeds. Taking the
275 displacements into account improves the departure statistics between measurements and ERA5 not only for temperature but
276 also wind and relative humidity (**Figure 10**).

277

278 For relative humidity, the improvement is confined to levels located below 250 hPa. Above this level, the relative humidity
279 is generally very low, making it difficult to detect any meaningful difference with respect to the ERA5 background.

26
27



28

280 It is also important to note that some stations, where the RMSE of the ascents do not show signals of improvement in
281 temperature, often still show improvement in humidity or wind (or vice versa).

282

283 Considering that early radiosonde observations make up a larger part of the total observations for the reanalysis in earlier
284 years, one might think that especially for these years the displacements are more relevant. The data investigation reveals that
285 improvements of the departure statistics are not greater for earlier ascents than for more recent ascents. The reason might be
286 that reanalysis fields before the satellite era are more strongly dependent on radiosondes. At these times few other upper-air
287 observations were available, and radiosonde data were assimilated assuming vertically straight ascents. However, the density
288 of the input data and the general quality of the reanalysis increased over the time, while the bias in measurements of the
289 uppermost levels decreased over time. Therefore, the relative importance of representation uncertainties, with respect to the
290 two other sources of uncertainties in the comparison (radiosonde instrumental uncertainties and ERA5 background
291 uncertainties), is larger for more recent ascents. **Figure 11** shows that considering the displacements is beneficial, although
292 to a lesser extent, also in the early days, when little upper air information other than radiosondes was available.

293

294 Finally, in **Figure 12** there are the results of a global comparison for the year 2000 - like the previous ones, but calculated for
295 all the available stations. A positive difference again indicates improvement due to taking the displacements into account.

296

297 To give a better insight, the differences of the RMSEs are also plotted on a map for the 150 hPa level in **Figure 13**. Warm
298 colours show improvement for the respective station by applying the displacements, cold colours show a deterioration.
299 Improvement clearly predominates for the majority of stations. Deteriorations in quality appear less frequent and of smaller
300 magnitudes than improvements.

301

302 **Figure 14** shows the difference of the ERA5 background eastward wind speed in the 1990s at the station location minus the
303 same wind speed at the displaced location. The differences are sizable in some regions. For example, the weaker wind speeds
304 above station locations in China would indicate systematically too high observed wind speeds. This effect is large enough to
305 explain some of the radiosonde wind minus background wind differences, as pointed out by Tenenbaum et al. (2022). This
306 stresses again the importance of avoiding position errors in historical radiosonde ascents. Without the adjustments, artificial
307 trends in wind speed from radiosondes would be introduced in some regions when switching from traditional to GNSS
308 radiosondes.

309



31

310 6. Evaluation with data assimilation experiments

311 Desroziers et al. (2005) proposed a method to diagnose uncertainty statistics of observations, in a data assimilation
312 framework. As indicated in their work, there are important assumptions associated with the approach. Bias contributions
313 aside, the overall level of uncertainties may be incorrect if, for example, there is significant correlation between observation
314 random uncertainties and random uncertainties of the background that is used in the data assimilation. A separation of scales
315 is indeed required in order to disentangle these two uncertainty components. Given the unique importance of radiosondes to
316 inform on the state of the stratosphere in a background obtained from data assimilation, such as in a reanalysis (e.g.,
317 Hersbach et al., 2020), there may be some components of the uncertainties (such as radiation) that are present, and possibly
318 correlated, in the background and the observations. For these reasons, we do not use Desroziers' diagnostics in order to
319 assign undisputable uncertainties to the radiosonde uncertainties. Instead, we use these diagnostics in order to detect any
320 changes in the observation uncertainties, which include instrument and representativity uncertainties, owing to the effect of
321 balloon drift.

322

323 To this end, we run two data assimilation experiments, using a simplified data assimilation setup. Simplifications are
324 required in order to make such an undertaking numerically affordable. Otherwise, so-called 'full' data assimilation
325 experiments, using all observations at the maximum resolution, are indeed too costly to conduct, if only for such an
326 evaluation. The simplified data assimilation setup is based on the ECMWF Integrated Forecasting System (IFS) cycle 48R1
327 configuration (ECMWF, 2023), using a octahedral reduced Gaussian grid with 159 wavenumbers, or approximately a
328 horizontal resolution of 69 km, instead of the ECMWF operational configuration which has a resolution of approximately 9
329 km at present. Also, similarly for affordability reasons, the experiments only assimilate conventional observations (no
330 satellite observations), the number of four-dimensional variational (4D-Var) minimizations is reduced from three to two, and
331 the analysis increments are at a resolution of approximately 210 km (instead of 39 km for ECMWF operations).

332

333 The first experiment is the control. It assimilates the radiosonde observations as vertical profiles. The second experiment
334 assimilates the radiosonde observations as slanted profiles, following the balloon trajectory, when it is available (otherwise
335 the data are assimilated as vertical profiles). The simplified data assimilation setup enables us to run these two experiments
336 for a duration of two months, 01 June - 31 July 1980.

337

338 We consider here the radiosonde observations that were assimilated in both experiments, to ensure no difference in results
339 may be caused by sampling differences. **Table 4** shows the statistics for these data. For the reasons mentioned earlier, the
340 interpretation of the table focuses on differences between the two experiments, and not on the absolute level of observation
341 uncertainties determined by Desroziers' diagnostics. Within 0.1 K, we find no detectable difference between the two
342 experiments for the pressure levels below 100 hPa. For pressures lower than 100 hPa, one finds that background departures

32
33



34

343 and estimated observation uncertainties are reduced in the experiment that assimilated the data along slanted profiles. This
344 result is obtained for radiosondes launched from land stations as well as radiosondes launched from ships.

345

346 The differences may appear as very small and could be discarded as non important, if it was not for the fact that reducing
347 such quantities is generally an impossible task, once observations were collected and processed already once. The present
348 findings demonstrate that it is possible to generate greater return, in terms of information content, through a reprocessing of
349 the observations. Furthermore, these are global statistics - see **Figure 15**. The previous sections indicated that results may
350 vary per launch site. Consequently, the improvements shown here, for global statistics, must hide some greater
351 improvements at some particular sites - see **Figure 16**.

352

353 **7. Discussion and conclusions**

354 The verification and evaluation results have shown quite clearly that if at all possible, balloon displacements should be taken
355 into account for all relevant data assimilation applications to minimise representation errors. Ignoring the possibility to
356 account for observation location errors on the 100 km scale would be anachronistic, when global or regional reanalysis data
357 sets approach spatial resolutions finer than 20 km.

358

359 The method to reconstruct the balloon position presented in this work is limited by a few assumptions and depends on the
360 vertical resolution of the available profiles, and the conformance of the weather balloons to modern ascent speeds. For the
361 applications tested, an attempt was made to obtain the best results globally, and a clear positive impact was found,
362 particularly when comparing to ERA5 in the early 2000s, although positive results were also found at other times (e.g.,
363 1980s). This is also consistent with other findings in similar settings where trajectory data are used to reduce representation
364 errors (e.g., Laroche, 2013).

365

366 The data assimilation experimental setup employed here is a simplified one, as compared to what may be used in a present-
367 day reanalysis configuration such as ERA5. Yet, we observe a positive impact of the balloon drift in terms of reducing the
368 background departures and the observation uncertainty, using Desroziers' diagnostics, for temperatures in the stratosphere.
369 We expect that the impact of using radiosondes at a displaced horizontal position would increase when the background
370 resolution is increased. Furthermore, we also expect that any positive impact of sonde displacement be amplified when
371 satellite observations are used alongside radiosondes. Owing to time and computational constraints, it was not possible to
372 investigate further these effects with full data assimilation experiments at higher horizontal resolution and using all available
373 information, but we note this would be a useful pursuit.

374

35
36



37

375 The results of the tests have shown that the method is successful in reconstructing displacements and improving the accuracy
376 of the atmospheric data. Whilst the additional information provided by the method may not always be a visible improvement
377 for individual comparisons, it is of significant value when the displacement changes the gridbox of the model being
378 compared. This has been demonstrated by improved means in the plots and better agreement between observations and
379 ERA5.

380

381 The value of improving radiosonde observations by reprocessing of the positions was evaluated by conducting reduced-
382 resolution data assimilation experiments, covering a two-month period in summer 1980. In the future, it would be desirable
383 that the impact of similar activities that seek to improve the observational record be more regularly evaluated in the
384 generation of downstream climate products. Such an evaluation should consider a longer time period and include the impact
385 on low-frequency variability in the products. For products such as reanalyses, obtained via data assimilation, this should
386 entail full-resolution Observing System Experiments (OSEs). For other types of climate products, including those powered
387 by new opportunities such as Artificial Intelligence or Machine Learning (e.g., Singh et al., 2022), it is important that
388 mechanisms be found to evaluate the impact of using the observations and how changes made in their handling affects the
389 outcome.

390

391 Further experimentation using observation data from the period 2000 - 2020 is crucial and is likely to produce more
392 compelling outcomes. The effective use of this method for informing future climate reanalysis is one of the main objectives.
393 As the world faces increasing challenges related to climate change, the importance of accurate atmospheric data and the
394 potential of new methods to improve it cannot be overstated. The use of improved position metadata with radiosonde
395 observations can account for previously unexplainable phenomena, demonstrating the potential of this method to shed new
396 light on atmospheric data analysis. In addition, the method has the potential to improve the accuracy of reanalyses and
397 climate predictions, which is crucial for the protection of future life.

398

399 To achieve the optimal representation of the data, precise details regarding time and location must be available for every
400 observation. One significant issue concerns the TAC format's transmission and storage of data, which often only includes a
401 nominal timestamp such as 00:00 UTC or 12:00 UTC. However, the actual launch of the respective balloon in most cases
402 took place 30-60 minutes earlier. The precise time difference from the nominal time is frequently unknown, therefore
403 displacement information cannot be utilised to its fullest extent. Since temperature can vary by more than 1 K/h in the
404 boundary layer just due to the diurnal cycle this issue should be addressed. There are well known examples where changes in
405 the sampling of the diurnal cycle introduced spurious trends into climate data products (Mears and Wentz, 2005). Whenever
406 possible, the precise launch time should be used. In cases where this information is not available for individual ascents, the
407 time difference between the nominal and actual launch can be determined from earlier or later ascents. Operators are

38
39



40

408 normally advised to minimise the variation throughout the launch procedure and, therefore, launch balloon sondes at the
409 same time every day.

410

411 Additional work to better understand the causes of variation in balloon ascent speeds (e.g., Zhang et al., 2019) could help
412 further improve the results. Also, given all the uncertainty sources, it could be possible to generate an ensemble of
413 trajectories for each ascent.

414 The same approach can be used to reprocess rocket or drop sondes, ozone sondes or any other in-situ sonde carried by the
415 wind, provided the necessary information is available. Taking into account the accurate balloon position would also be
416 beneficial when comparing radiosonde observations with GNSS radio occultation (RO) observations (Gilpin et al. 2018).
417 While the slanted profile of the RO data is considered, radiosonde data is frequently presumed to move vertically only.

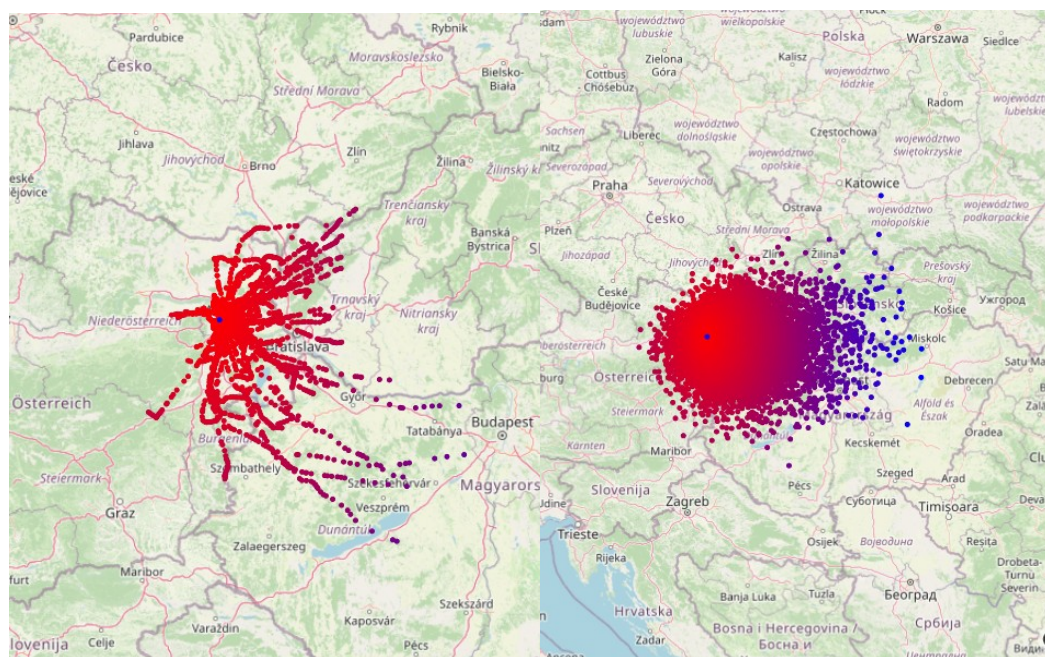
418

419 In conclusion, the development and testing of the method for reconstructing displacements based on the reversed calculation
420 of wind speed and direction shows promising results. The results presented in this paper suggest taking balloon
421 displacements into account when producing meteorological or climatological data based on upper-air in situ balloon-borne
422 observations.



43

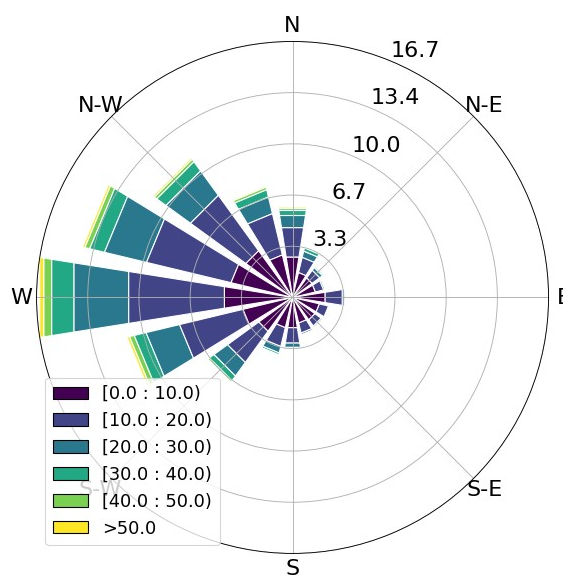
424 **Appendices**



425

426

© OpenStreetMap contributors 2023. Distributed under the Open Data Commons Open Database License (ODbL) v1.0.



427

428

429

430

431

432

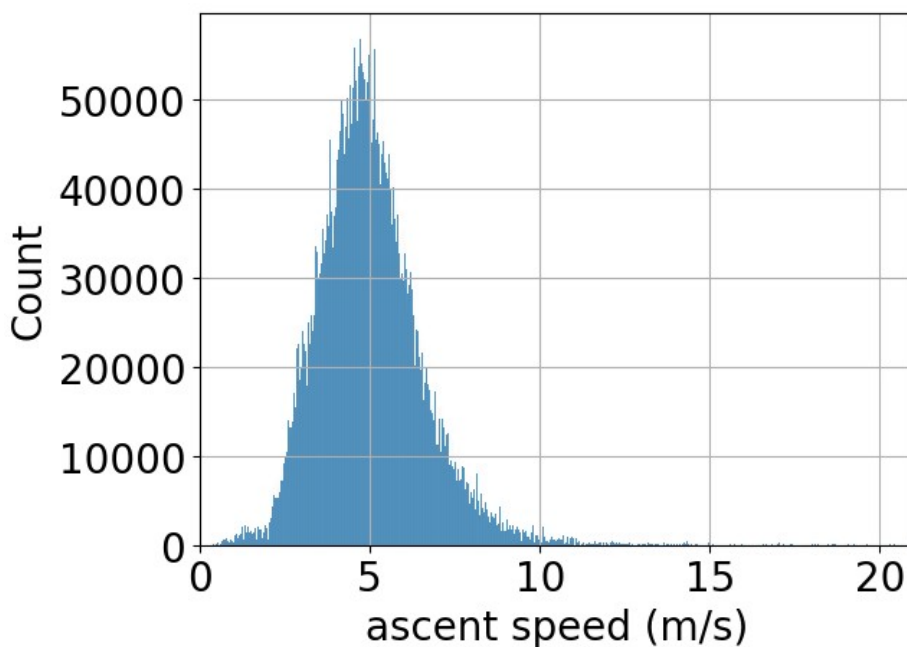
Figure 1: Balloon displacements for station Vienna Hohe Warte, Austria (WIGOS ID 0-20001-0-11035, central blue dot) red to blue with increasing distance. Note the area covered is non-isotropic around the launch site. Left panel: Trajectories of all radiosonde ascents during the year 2000. Right panel – maximum displacements of all available ascents for all years between 1950 and 2021. Lower panel: windrose of Vienna Hohe Warte station for all available wind data. Colour indicates wind speed [m/s], radius indicates frequency distribution [%] of wind direction (sectors) and wind speed (colors).

44

45

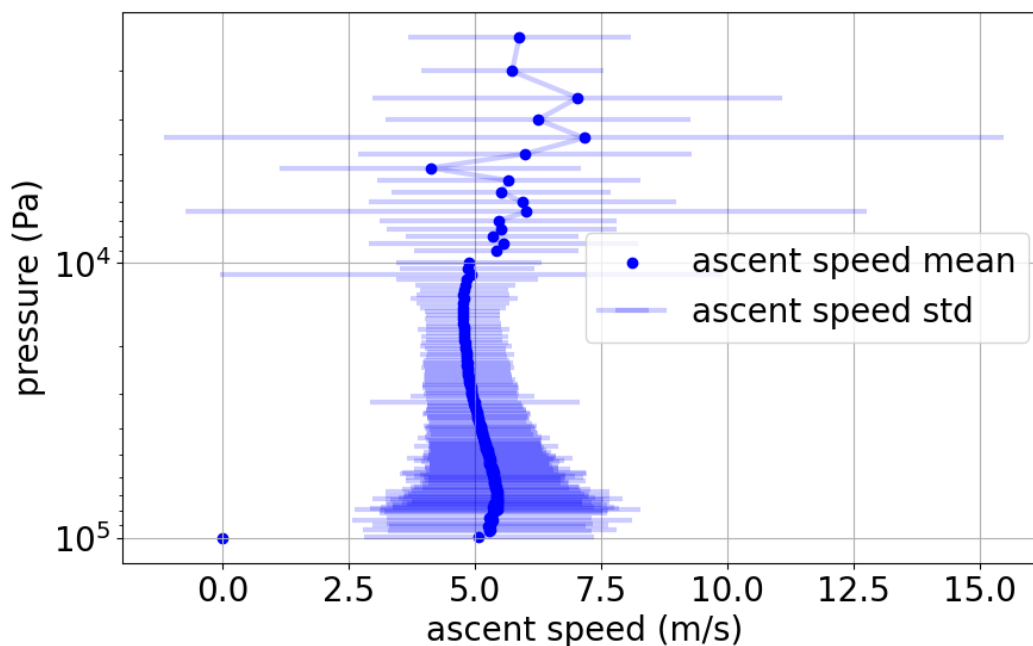


46



433

434 **Figure 2: The observed ascent speeds from a sample of approximately 10 million BUFR encoded observations with known altitude**
435 **time series in 2020.**



436

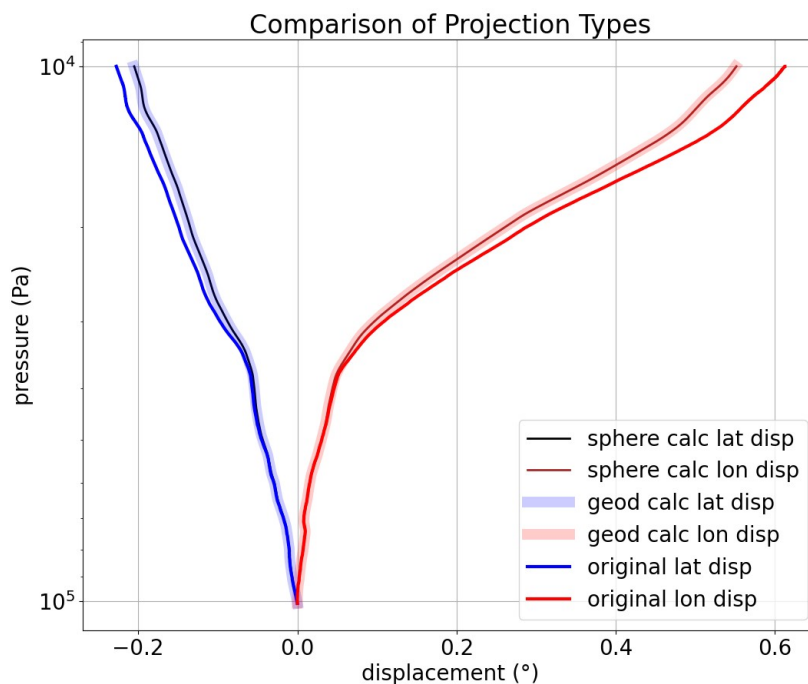
437 **Figure 3: Mean ascent speed with standard deviation bars for all radiosonde ascents from Riverton USA, in 2020, derived from**
438 **high resolution BUFR data.**

47

48

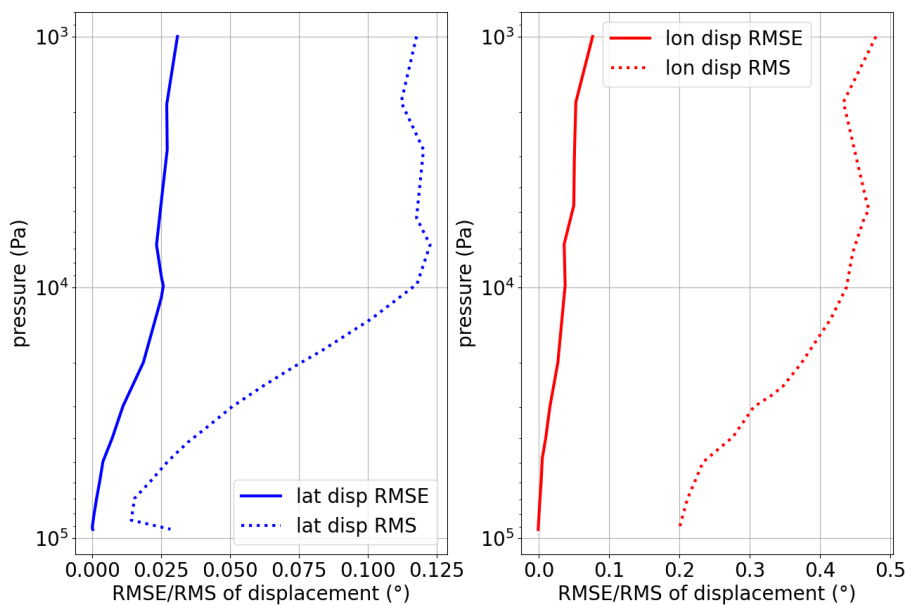


49



439
 440
 441
 442

Figure 4: Calculated displacements (black and brown for spherical earth, thick light blue and red for WGS84). Observed displacements stored in BUFR displacements (blue and red) are included for comparison. Tallahassee, Florida - USA 2020.05.31 23:19:00



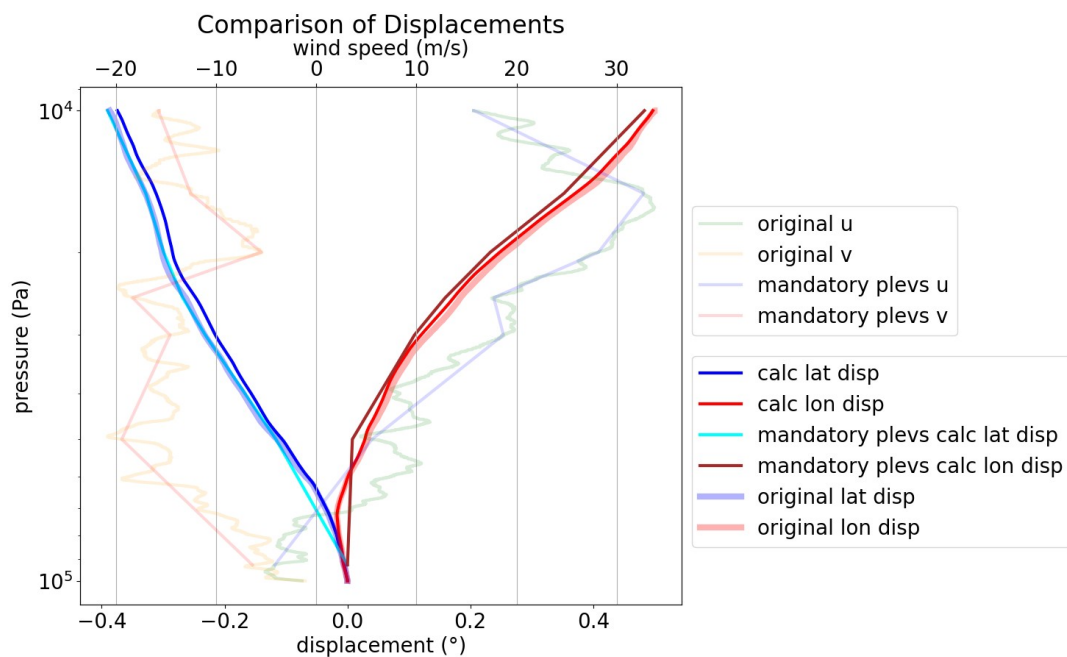
443
 444
 445
 446

Figure 5: RMS of latitude (blue dotted) and longitude (red dotted) displacements and RMSE between observed (from GPS) and modelled displacements (solid blue and solid red, respectively). The samples contain all BUFR encoded ascents in the summer months of 2020 (more than 10000).

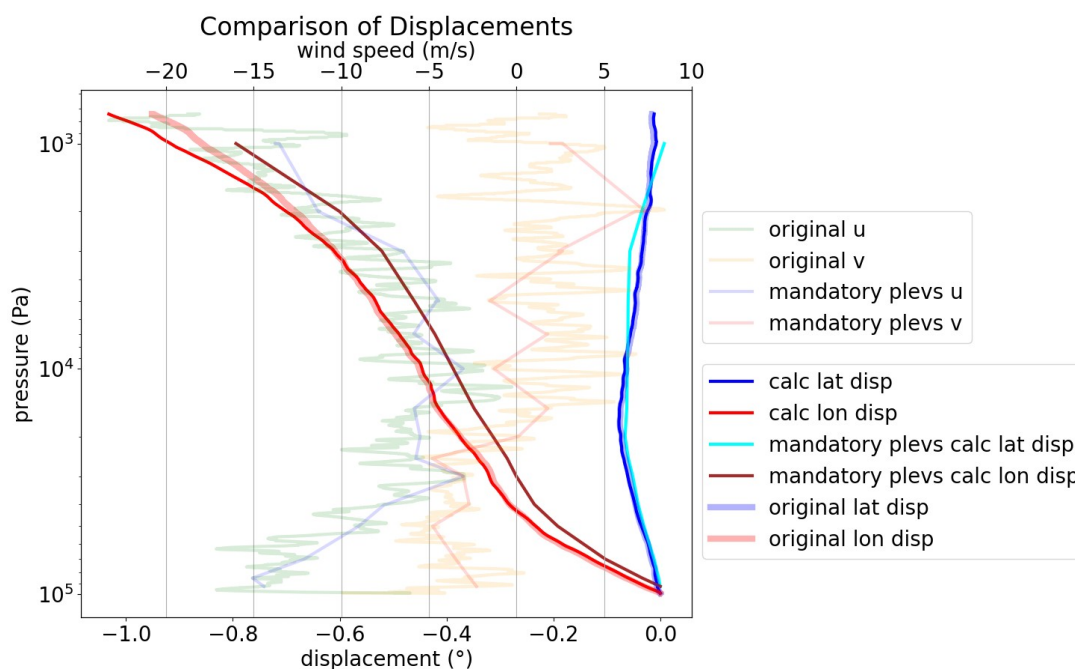
50
 51



52



447
 448 **Figure 6: Vertical profiles of displacements (starting at zero at surface), calculated from observed winds (thin lines) or taken from**
 449 **BUFR thick light lines. The profiles of observed wind (thin light colors) are plotted to the upper x axis - Green Hill, Tennessee -**
 450 **USA 31.05.2020 23:00:00**
 451



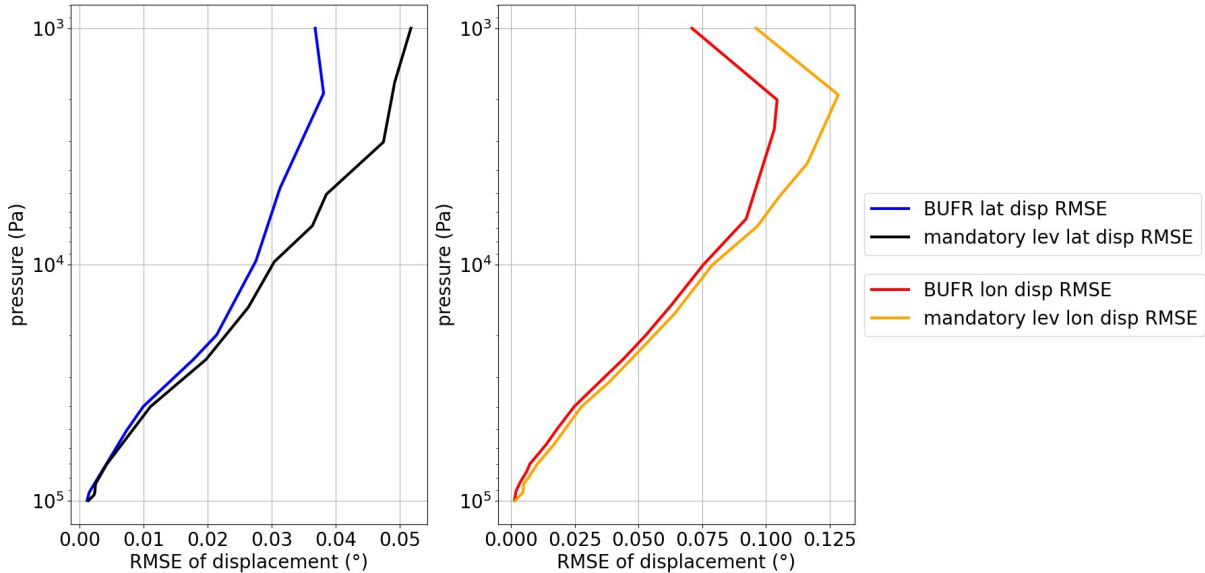
452
 453 **Figure 7: Vertical profiles of displacements (starting at zero at surface), calculated from observed winds (thin lines) or taken from**
 454 **BUFR thick light lines. The profiles of observed wind (thin light colors) are plotted to the upper x axis - St. Paul Island Airport,**
 455 **Alaska - USA 2020.05.31 23:01:00**

53
 54



55

456



457

458

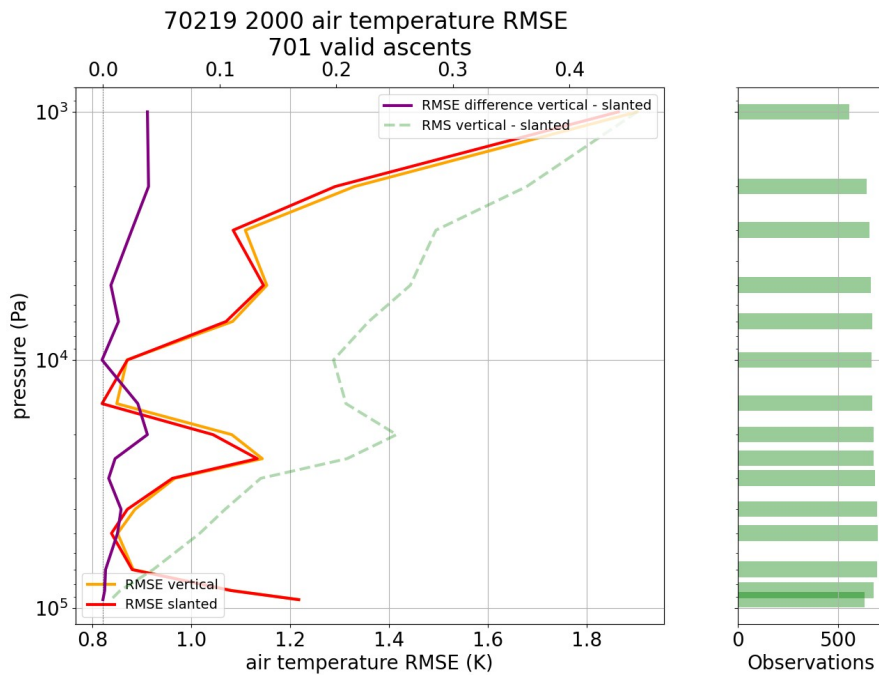
459

460

461

462

Figure 8: RMSE between observed and modelled displacements of latitude (left panel) and longitude (right panel), averaged over all stations available in October 2014, one of the first months with a sizable number of high-resolution BUFR encoded profiles. Blue and red are RMSE profiles obtained by using the full vertical resolution of BUFR observations, black and orange are RMSE profiles, and obtained by using only mandatory level information.



463

464

465

466

467

468

Figure 9: Bethel Airport, Alaska all 2020 ascents. RMSE (obs - ERA5) of base coordinate temperatures minus sonde temperatures (orange) and RMSE (obs - ERA5) of displaced temperatures minus sonde temperatures (red), also RMS of displaced minus base (green dashed) to show the magnitude of difference between base and displaced temperatures. Positive difference between orange and red graphs (purple line, upper x axis) shows improvement due to more accurate balloon position. Green bars on the right indicate sample sizes at different levels.

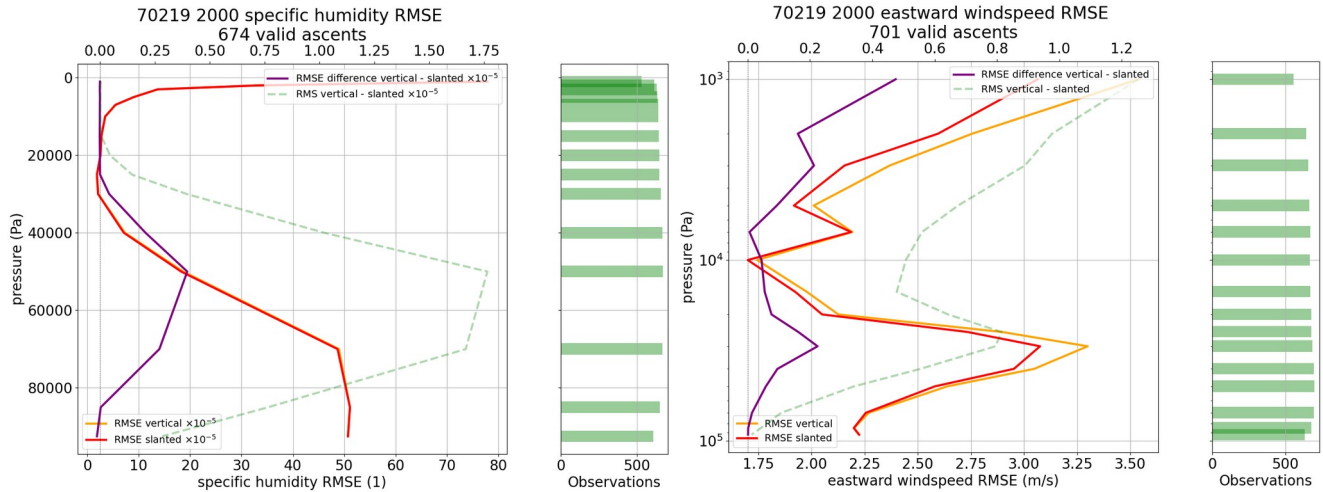
56

57



58

469



470

471

472

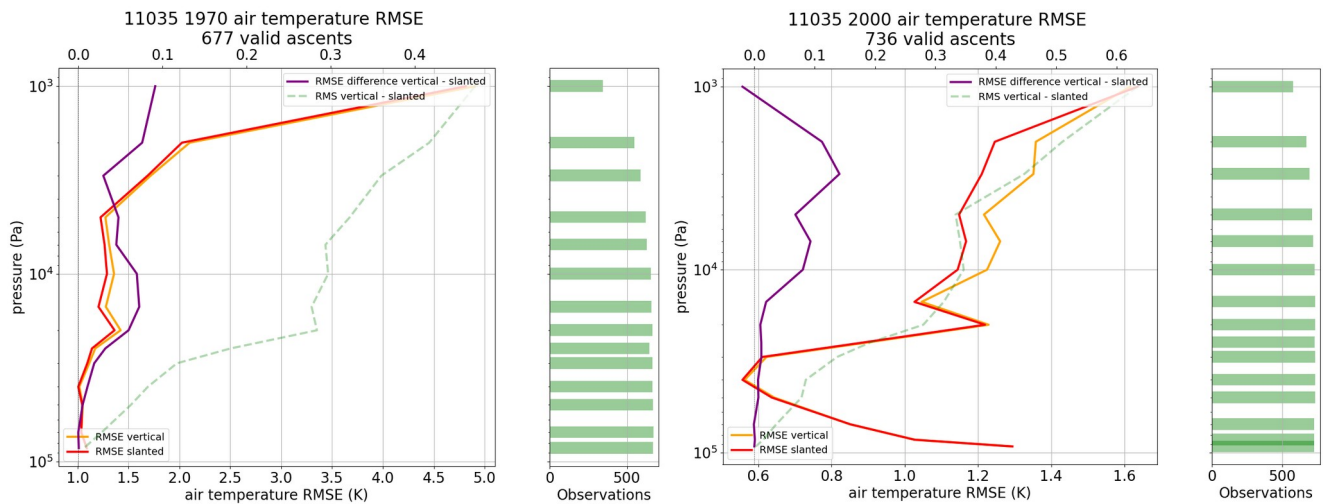
473

474

475

Figure 10: Bethel Airport, Alaska all 2020 ascents. left: RMSE (obs - ERA5) of vertical specific humidity minus sonde specific humidity (orange) and RMSE (obs - ERA5) of slanted specific humidity minus sonde specific humidity (red). right: RMSE (obs - ERA5) of vertical eastward wind minus sonde eastward wind (orange) and RMSE (obs - ERA5) of slanted eastward wind minus sonde eastward wind (red). Positive difference between orange and red graphs (purple line, upper x axis) shows improvement due to more accurate balloon position.

476



477

478

479

480

481

Figure 11: Vienna Hohe Warte, Austria - Left: 1970 all ascents, Right: 2020 all ascents. Different x-axes scales are used. RMSE (obs - ERA5) of vertical temperature minus sonde temperature (orange, lower x-axis) and RMSE (obs - ERA5) of slanted temperature minus sonde temperature (red, lower x-axis). Positive difference between orange and red graphs (purple line, upper x axis) shows improvement due to more accurate balloon position.

59

60



61

482

483

484

485

486

487

488

489

490

491

492

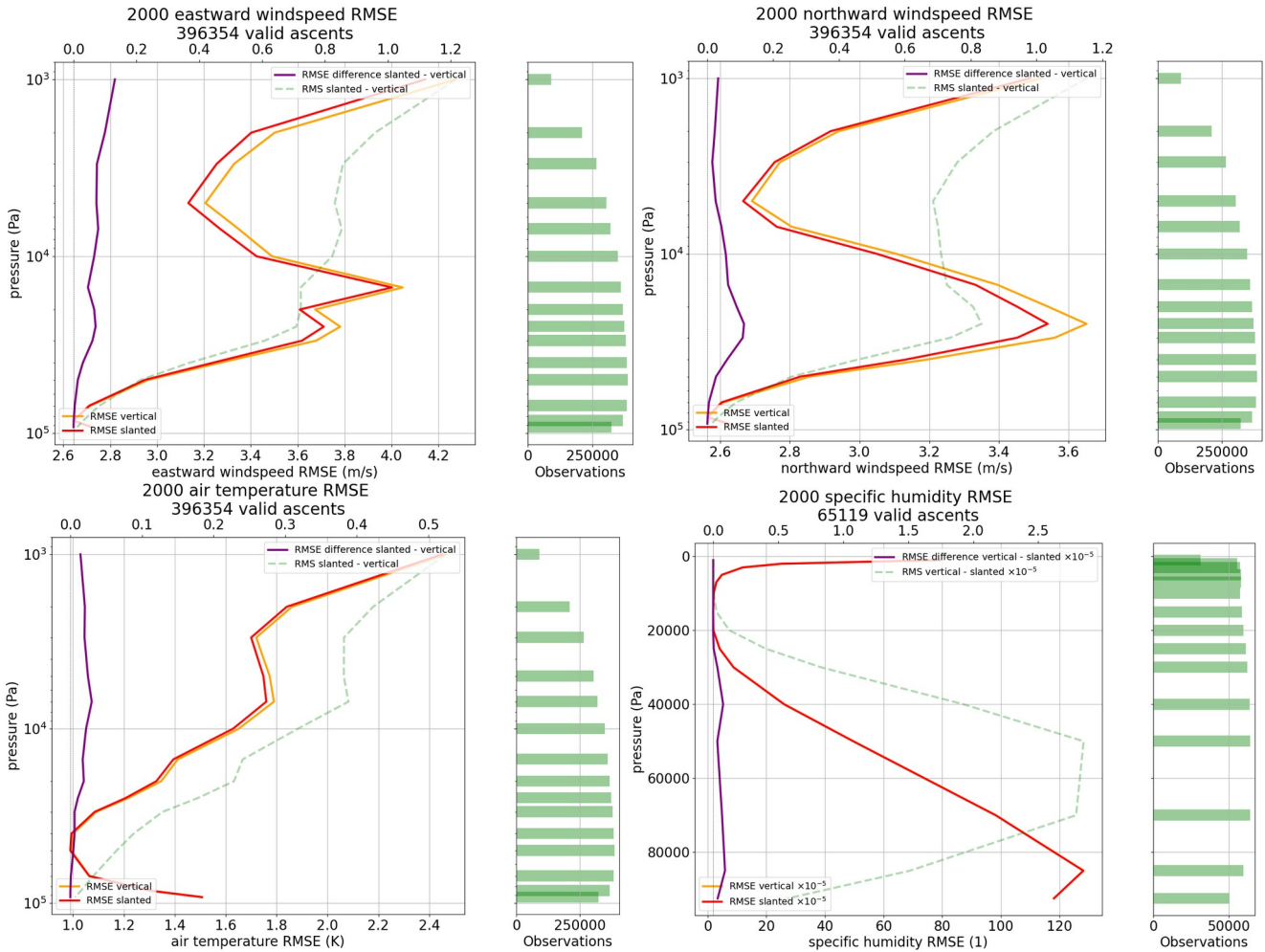


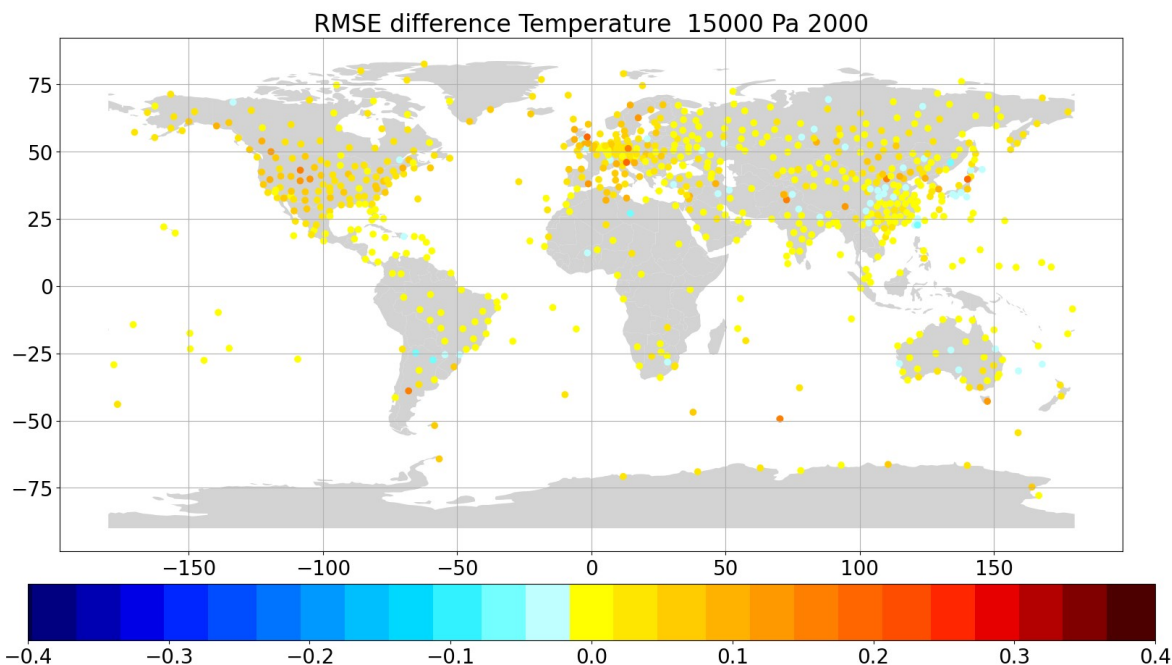
Figure 12: Global RMSE (obs - ERA5 background) assuming vertical ascents (orange) and RMSE (obs - ERA5 background) from reconstructed slanted ascents (red), calculated from all available ascents of year 2000. The differences between orange and red graphs (purple line, upper x axis) shows how much the better balloon position improved the temperature data (positive = improvement). The “RMS vertical - slanted” (green dashed line, upper x axis) indicates how much the ERA5 background varies on average between the vertical and slanted balloon profiles. - Top left: u wind component; Top right: v wind component; Bottom left: temperature; Bottom right: specific humidity.

62

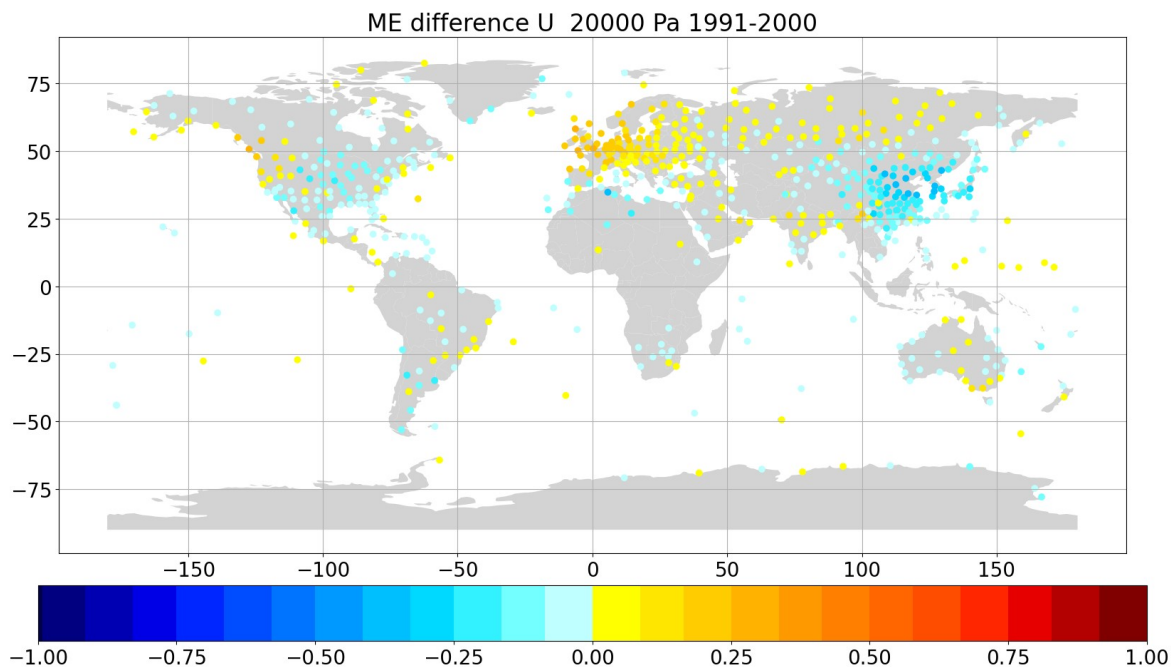
63



64



494
495 **Figure 13: Global stations difference of temperature [K] observation RMSE (obs - ERA5) when compared to background at**
496 **station coordinates minus the temperature observation RMSE (obs - ERA5) when compared to background at displaced position -**
497 **Positive values indicate improvement due to more accurate balloon position. All available observations at 150 hPa averaged over**
498 **all ascents in the year 2000.**

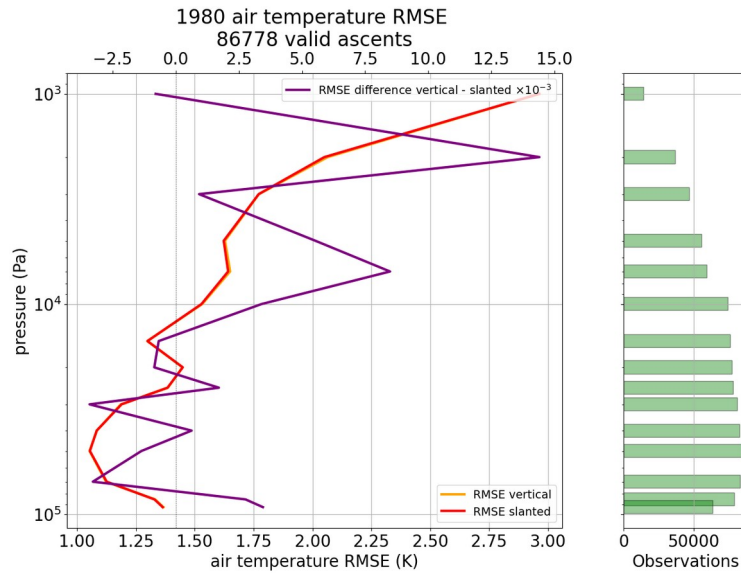


499
500 **Figure 14: Mean u wind [m/s] difference obs - ERA5 background at station position minus obs - ERA5 background at displaced**
501 **position. All available values on 200 hPa of years 1991 - 2000.**

65
66

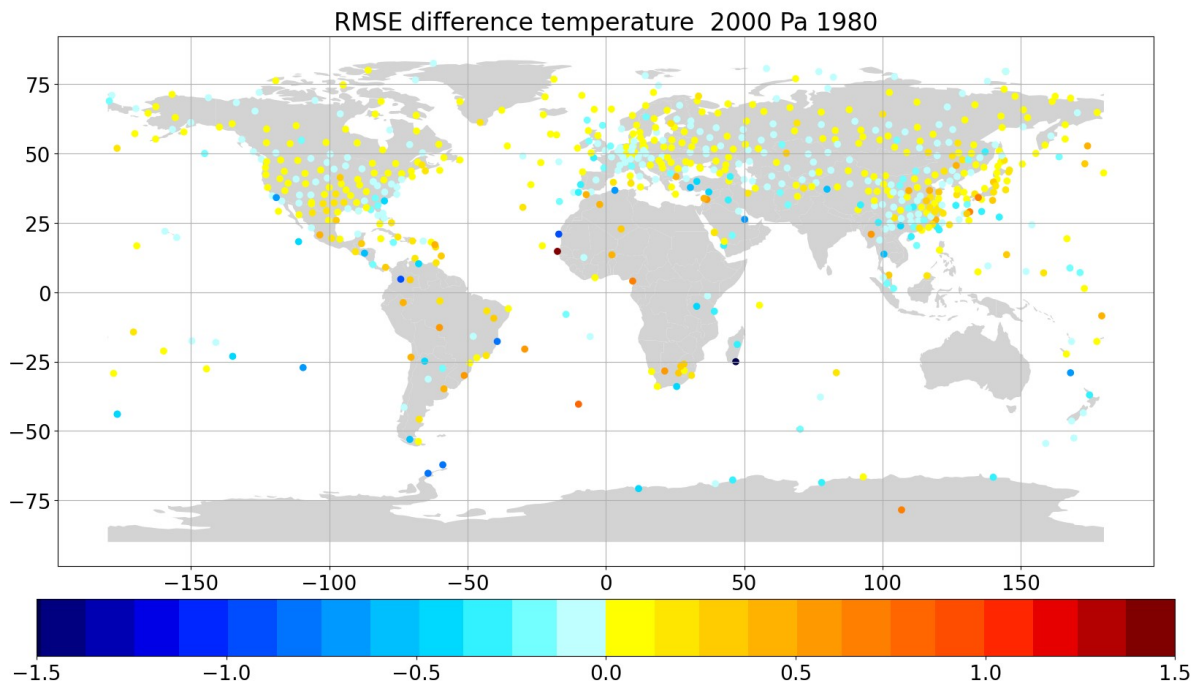


67



502

503 **Figure 15: Air temperature obs-bg RMSE difference for experiment “vertical” (orange) and for experiment “slanted” (red). The**
 504 **difference of differences (orange-red) yields the purple line, upper x axis). Positive values indicate improvement due to more**
 505 **accurate balloon position. All available stations on mandatory pressure levels between 1980.06.01-1980.07.31.**



506

507 **Figure 16: Air temperature obs-bg RMSE [K] difference of experiment “vertical” minus RMSE of experiment “slanted”. Positive**
 508 **values indicate improvement due to usage of more accurate balloon position. All available stations on 20 hPa between 1980.06.01-**
 509 **1980.07.31.**

68

69



70

510 **Formula 1, 2: Calculation of the vertical gradient of temperature. See Table 1.**

511
$$\Gamma_{(p)} = \frac{\delta T}{\delta z} = \frac{\delta T}{\delta p} \frac{\delta p}{\delta z} = \frac{-\delta T}{\delta p^\kappa} \frac{\delta p^\kappa}{\delta p} \frac{\delta p}{\delta z} \quad (1)$$

512
$$\Gamma_{(p)} = \frac{-\delta T}{\delta p^\kappa} \frac{p^\kappa}{T} \frac{\kappa g}{R_d} \quad (2)$$

513

514

515 **Formula 3: Calculation of layer height. See Table 1.**

516
$$\Delta z_{(i \rightarrow i+1)} = \frac{T_i}{\Gamma_i} \left(\frac{p_{i+1}}{p_i} \right)^{\frac{-\Gamma_i R_d}{g} - 1} \quad (3)$$

517

518

519

Table 1: Height profile calculation. Explanation of all used variables.

Symbol	Description	Unit	Data source
Γ	temperature lapse rate	[K/m]	observed variable
p	pressure	[Pa]	observed variable
T	temperature	[K]	observed variable
Δz	layer height	[m]	calculated variable
κ	isentropic expansion factor	[1]	$\kappa = R/c_p$
C_p	specific heat capacity of air at constant pressure	[J/kg/K]	constant (1005.7)
R_d	gas constant for dry air	[J/kg/K]	constant (286.7)
g	standard gravity	[m/s ²]	constant (9.80665)

520

521

71

72



73

522 **Formula 4: Transport of the balloon with the wind. See Table 2.**

$$523 \quad \vec{s}_{(i+1)} = \frac{\vec{u}_{(i \rightarrow i+1)} * \Delta z_{(i \rightarrow i+1)}}{W_{balloon}} \quad (4)$$

524

525

526 **Table 2: Time interval calculation. Explanation of all used variables.**

Symbol	Description	Unit	Data source
\vec{s}	distance travelled	[m]	0 at i = 0, lon for u, lat for v
\vec{u}	wind	[m/s]	observed variable, u and v components of wind
Δz	layer height	[m]	calculated variable
w	rate of ascension	[m/s]	5, prescribed variable

527

528

529 **Table 3: Ascent speed percentiles for a sample of 10.000.000 observations with known altitude time series in 2020.**

Percentile	Value	Unit
1	2.05	[m/s]
5	2.82	[m/s]
25	4.01	[m/s]
75	5.85	[m/s]
95	7.74	[m/s]
99	10.09	[m/s]

530



76

532 **Table 4: Statistics for the radiosonde observations actively used by both data assimilation experiments (vertical and slanted),**
 533 **separating between radiosondes launched from land stations and radiosondes launched from ships. P indicates the pressure (hPa),**
 534 **RSD indicates the robust standard deviation of background departures (i.e., before assimilation), SIGO indicates the estimated**
 535 **observation uncertainty (see text for details), and N indicates the data count. Results that differ between the two experiments are**
 536 **shown in bold and underlined. Observations that were used by only either one of the two experiments are excluded from these**
 537 **statistics.**

Pressure level range	P ≥ 500 hPa		500 hPa > P ≥ 100 hPa		100 hPa > P ≥ 1 hPa	
Experiment	Vertical	Slanted	Vertical	Slanted	Vertical	Slanted
Radiosondes from land stations						
RSD	1.2 K	1.2 K	1.3 K	1.3 K	<u>2.1 K</u>	<u>2.0 K</u>
SIGO	1.1 K	1.1 K	1.2 K	1.2 K	<u>2.1 K</u>	<u>2.0 K</u>
N	31,027,909	31,027,909	30,229,363	30,229,363	1,358,298	1,358,298
Radiosondes from ships						
RSD	1.2 K	1.2 K	1.2 K	1.2 K	<u>1.6 K</u>	<u>1.5 K</u>
SIGO	1.1 K	1.1 K	1.2 K	1.2 K	<u>1.8 K</u>	<u>1.6 K</u>
N	838,265	838,265	669,655	669,655	34,709	34,709

539

540



79

541 **Code and data availability**

542 Radiosonde data used in the present work are available from <https://doi.org/10.7289/V5X63K0Q> (IGRA) and
543 <https://doi.org/10.24381/cds.f101d0bf> (C3S CDS) and the University of Wyoming Atmospheric Science Radiosonde
544 Archive (<https://weather.uwyo.edu/upperair/bufrroaob.shtml>). Climate reanalysis data (ERA5) are available from
545 <https://doi.org/10.24381/cds.bd0915c6>. The code discussed in this paper is available from
546 <https://doi.org/10.5281/zenodo.8421009>.

547 **Author contribution**

548 Ulrich Voggenberger and Leopold Haimberger designed the method to estimate balloon positions. Ulrich Voggenberger
549 developed the code and optimised the estimations and calculations with further input from Federico Ambrogio. Ulrich
550 Leopold Haimberger and Ulrich Voggenberger verified and evaluated the results based on ERA5 data. Paul Poli ran the data
551 assimilation experiments and evaluated the results in section 6. Ulrich Voggenberger prepared the manuscript with
552 contributions from all co-authors.

553 **Competing interests**

554 The contact author has declared that none of the authors has any competing interests.

555 **References**

- 556 Alexander, P., and De La Torre, A.: Uncertainties in the measurement of the atmospheric velocity due to balloon-
557 gondola pendulum-like motions. *Adv. Space Res.*, 47 (4):736-739, <https://doi.org/10.1016/j.asr.2010.09.020>, 2011.
- 558 Crutcher, H. L.,: Distribution of radiosonde errors. NOAA Tech. Rep. Environmental Data and Information Service
559 (EDIS), 32, https://repository.library.noaa.gov/view/noaa/30830/noaa_30830_DS1.pdf, 1979.
- 560 Dabberdt, W. F., and Turtiainen, H.: Observations platforms: Radiosondes, in *Encyclopedia of Atmospheric Sciences*
561 (Second Edition), eds. G. R. North, J. Pyle, F. Zhang, Academic Press, pp 273-284, ISBN 9780123822253.
562 <https://www.sciencedirect.com/referencework/9780123822253/encyclopedia-of-atmospheric-sciences>, 2015.
- 563 Desroziers, G., Berre L., Chapnik B., and Poli, P.: Diagnosis of Observation, Background and Analysis-Error
564 Statistics in Observation Space. *Quarterly Journal of the Royal Meteorological Society* 131, no. 613 (October 1,
565 2005): 3385–96. <https://doi.org/10.1256/qj.05.108.>, 2005.

80
81



82

- 566 Durre, I., Yin, X., Vose, R. S., Applequist, S., Arnfield, J., Korzeniewski, B., and Hundermark, B.: Integrated Global
567 Radiosonde Archive (IGRA), Version 2. NOAA National Centers for Environmental Information.
568 <https://doi.org/10.7289/V5X63K0Q>, 2016.
- 569 Dutton, J. A.: The ceaseless wind: An Introduction to the Theory of Atmospheric Motion. Dover Publications, New-
570 York, 617 pp., ISBN:978-0486495033, <https://doi.org/10.1029/88EO01137>, 1986.
- 571 ECMWF: IFS Documentation CY48R1. <https://www.ecmwf.int/en/publications/ifs-documentation>, last access 25 Oct
572 2023
- 573 Favà, V., Curto, J. J., and Gilabert, A.: Thermodynamic model for a pilot balloon, Atmos. Meas. Tech. Discuss.
574 [preprint], <https://doi.org/10.5194/amt-2021-206>, 2021.
- 575 Gilpin, S., Rieckh, T., and Anthes, R.: Reducing representativeness and sampling errors in radio occultation–
576 radiosonde comparisons, Atmos. Meas. Tech., 11, 2567–2582, <https://doi.org/10.5194/amt-11-2567-2018>, 2018.
- 577 Hersbach, H., Bell, B., Berrisford, P, et al.: The ERA5 global reanalysis. Q J R Meteorol Soc. 2020; 146: 1999–2049.
578 <https://doi.org/10.1002/qj.3803>, 1999.
- 579 ICAO Standard Atmosphere - ISA <https://www.foehnwall.at/meteo/isa.html>, last access 25 Oct 2023
- 580
- 581 Ingleby, B., Isaksen, L., Kral, T., Haiden, Th., and Dahoui, M.: Improved use of atmospheric in situ data. ECMWF
582 Newsletter 155. <https://doi.org/10.21957/cf724bi05s>, 2018.
- 583 Kitchen, M.: Representativeness errors for radiosonde observations. Q. J. R. Meteorol. Soc., **115**: 673-700.
584 <https://doi.org/10.1002/qj.49711548713>, 1989.
- 585 Laroche, S., and Sarrazin, R.: Impact of Radiosonde Balloon Drift on Numerical Weather Prediction and Verification.
586 Weather and Forecasting, 28 (3), 772–782. <https://doi.org/10.1175/waf-d-12-00114.1>, 2013.
- 587 Mears, C. A., and Wentz, F. J.: The effect of diurnal correction on the satellite-derived lower tropospheric
588 temperature. Science, 309, 1548–1551. <https://doi.org/10.1126/science.1114772>, 2005.
- 589 Murillo, J., Mejia, J., Galvez, J., Orozco, R., and Douglas, M.: Quality control of pilot balloon network data for
590 climate monitoring. Amer. Meteorol. Soc. 15th Conf. Appl. Clim., 13th Symp. Meteorol. Obs. Instr., **JP1.30** ,
591 <https://api.semanticscholar.org/CorpusID:56365106>, 2005.
- 592 OpenStreetMap: OpenStreetMap® is open data, licensed under the Open Data Commons Open Database License
593 (ODbL) by the OpenStreetMap Foundation (OSMF). You are free to copy, distribute, transmit and adapt our data, as
594 long as you credit OpenStreetMap and its contributors. If you alter or build upon our data, you may distribute the
595 result only under the same licence. The full legal code explains your rights and responsibilities. Our documentation is
596 licensed under the Creative Commons Attribution-ShareAlike 2.0 license (CC BY-SA 2.0). Available from
597 <https://planet.openstreetmap.org>, 2023.
- 598 Seidel, D. J., Sun, B., Petty, M., and Reale, A.: Global radiosonde balloon drift statistics, J. Geophys. Res., 116,
599 D07102, <https://doi.org/10.1029/2010JD014891>, 2011.

83
84



85

600 Singh, M., Kumar, B., Chattopadhyay, R., Amarjyothi, K., Sutar, A.K., Roy, S., Rao, S.A., and Nanjundiah, R.S.:
601 Artificial intelligence and machine learning in earth system sciences with special reference to climate science and
602 meteorology in South Asia. *Current Sci.*, **122** (9), <https://doi.org/10.18520/cs/v122/i9/1019-1030>, 2022.

603 Steinacker, R., et al.: Unstationary aspects of Föhn in a large valley. *Meteorology and Atmospheric Physics* volume
604 92, pages 255–284 (2006). <https://doi.org/10.1007/s00703-005-0134-y>, 2005.

605 Stohl, A.: Computation, accuracy and applications of trajectories - A review and bibliography, *Atmos. Env.*, **32** (6),
606 [https://doi.org/10.1016/S1352-2310\(97\)00457-3](https://doi.org/10.1016/S1352-2310(97)00457-3). 1998

607 Tenenbaum, J., Williams, P.D., Turp, D., Buchanan, P., Coulson, R., Gill, P.G., et al.: Aircraft observations and
608 reanalysis depictions of trends in the North Atlantic winter jet stream wind speeds and turbulence. *Quarterly Journal*
609 *of the Royal Meteorological Society*, 148(747), 2927–2941. <https://doi.org/10.1002/qj.4342>, 2022.

610 Tschannett, S.: Objektive hochaufgelöste Querschnittsanalyse. Diplomarbeit, Univ. Wien,
611 <https://www.univie.ac.at/img-wien/>, 2003.

612 WMO: Guide to Instruments and Methods of Observation Volume I: Measurement of Meteorological Variables ,
613 Commission for Instruments and Methods of Observation (CIMO) Guide, WMO Pub. 8. Available from
614 <https://library.wmo.int/records/item/41650-guide-to-instruments-and-methods-of-observation>, 2021.

615 Zhang, J., Chen, H., Zhu, Y., Shi, H., Zheng, Y., Xia, X., Teng, Y., Wang, F., Han, X., Li, J., et al.: A Novel Method
616 for Estimating the Vertical Velocity of Air with a Descending Radiosonde System. *Remote Sens.* **11**, 1538.
617 <https://doi.org/10.3390/rs11131538>, 2019.

618

86
87